

## Crystal Growth

International Edition: DOI: 10.1002/anie.201704499

German Edition: DOI: 10.1002/ange.201704499

## Fractal MTW Zeolite Crystals: Hidden Dimensions in Nanoporous Materials

HPSTAR  
471-2017

Lei Wang, Sheng-cai Zhu, Mei-kun Shen, Hai-wen Tian, Song-hai Xie, Hong-bin Zhang, Ya-hong Zhang, and Yi Tang\*

**Abstract:** Screw dislocation structures in crystals are an origin of symmetry breaking in a wide range of dense-phase crystals. Preparation of such analogous structures in framework-phase crystals is of great importance in zeolites but is still a challenge. On the basis of crystal-structure solving and model building, it was found that the two specific intergrowths in MTW zeolite produce this complex fractal and spiral structure. With the structurally determined parameters (spiral pitch  $h$ , screw angle  $\theta$ , and spatial angle  $\psi$ ) of Burgers circuit, the screw dislocation structure can be constructed by two different dimensional intergrowth sections. Thus the reported complexity of various dimensions in diverse crystals can be unified.

In the prosperous field of nanoscience, a major challenge is to fabricate intricate mesostructured crystalline materials with a desired architecture, morphology, and dimensions. Among various fascinating phenomena in nature, fractal and spiral structures have been the evergreen topics in fields from crystallography to materials science for their intriguing contributions to both fundamental research and practical applications. The natural world we live in teems with a plenty of branching structures (for example, snowflakes, trees, and galaxies). The recursive division of branches in the networks is treated as a self-similarity in fractal geometry. Additionally, the branching patterns are assembled by these fractal structures following a self-similarity law. On the other hand, the pivot to form spiral structure of crystal lies in the generation of a screw dislocation to break the symmetry of crystal growth and promote the anisotropic nanostructures. Such dislocation structures have been widely captured in dense-phase materials, such as metal oxides and alloy compounds,<sup>[1]</sup> ceramics,<sup>[2]</sup> carbon nanotubes,<sup>[3]</sup> and even ice.<sup>[4]</sup>

Comparatively, in framework materials, the complex dimension can be individually established: 1) a hierarchal

architecture formed by self-repeating pillared MFI<sup>[5]</sup> or rational intergrowth of FAU nanosheets,<sup>[6]</sup> and 2) a spiral structure in which spiral contour can be observed on the flat surface of various crystals, for instance, LTA, STA-7 (SAV), CHA/AEI, ZnPO<sub>4</sub>-Sodalite, and ZnPO<sub>4</sub>-Faujasite. In fact, although the screw dislocation core structure was predicted on the atomic scale of the LTA zeolite by Walker and co-workers,<sup>[7]</sup> the real nature of these frameworks remain elusive. Importantly, the high symmetry of these framework materials make the screw structure easy to be fused, causing the screw dislocation structure to be embedded in the bulky crystal. MTW zeolite is known for its catalytic properties to be a useful solid-acid catalyst.<sup>[8]</sup> MTW zeolite is composed of butterfly building unit (5<sup>4</sup>6<sup>1</sup>) layers, and the butterfly building layers stack into a 3D framework along the  $a$  axis by sharing four-membered ring structure. It often exists as intergrown polymorphs of two end-members of monoclinic (stacking sequence: ABCABC,  $C2/c$ ,  $a = 24.86 \text{ \AA}$ ,  $b = 5.01 \text{ \AA}$ ,  $c = 24.33 \text{ \AA}$ ,  $\beta = 107.7^\circ$ ) and orthorhombic phases (stacking sequence: ABABAB,  $Pm\bar{c}n$ ,  $a = 24.30 \text{ \AA}$ ,  $b = 23.70 \text{ \AA}$ ,  $c = 5.01 \text{ \AA}$ ). Remarkably, some other twinning behaviors, for example, the hexagonal star shape,<sup>[9]</sup> are also found apart from this polymorph twinning, but the origin still remains elusive. Herein, we successfully solve the crystal boundary in the branching hexagonal star of MTW zeolite with full connectivity, which is crucial in directing the evolution of regular morphology of the hexagonal star. By the combination of two intergrowths along  $\langle 310 \rangle$  and  $\langle 100 \rangle$  directions, the unique screw dislocation core structure can be achieved by above collaborative growth behaviors in two different dimensions. Thanks to the one-dimensional channel system of zeolite MTW, the unique pore direction can be adopted as dimensional indicator. Owing to the lower symmetry of the MTW framework, the segments around the screw dislocation cannot fuse into a bulky crystal for structure mismatching, which is different from that in the higher symmetry system (such as LTA, CHA/AEI). Furthermore, the phenomena in the framework materials with different symmetries can be unified and interpreted by the following conceptual structure.

In a typical synthesis, the reaction was performed by hydrothermal method with a diquatery ammonium type organic structure-directing agent (OSDA) C<sub>4</sub>H<sub>8</sub>(CH<sub>3</sub>)N<sup>+</sup>-C<sub>5</sub>H<sub>10</sub>-N<sup>+</sup>(CH<sub>3</sub>)C<sub>4</sub>H<sub>8</sub> (abbreviated as 1,5-MPP hereafter; Supporting Information, Figures S1, S2) containing siliceous gel. And then a different type and concentration of aluminum or boron sources was selectively added into the above gel to control the supersaturation level of the system. Once a homogenous gel formed, it was transferred into a Teflon-lined autoclave and hydrothermally treated at 433 K for

[\*] L. Wang, M. Shen, H. Tian, S. Xie, H. Zhang, Prof. Y. Zhang, Prof. Y. Tang  
Department of Chemistry, Shanghai Key Laboratory of Molecular Catalysis and Innovative Materials, Laboratory of Advanced Materials, and Collaborative Innovation Centre of Chemistry for Energy Materials, Fudan University  
Handan Rd. 220, Shanghai 200433 (P.R. China)  
E-mail: yitang@fudan.edu.cn  
S. Zhu  
Center for High Pressure Science and Technology Advanced Research (HPSTAR)  
Shanghai 201203 (P.R. China)

Supporting information and the ORCID identification number(s) for the author(s) of this article can be found under:  
<https://doi.org/10.1002/anie.201704499>

3 days under autogenous pressure statically. As exhibited in Figure 1, the crystallization of MTW zeolite can be divided into three regimes in its phase diagram referring to evolution of crystal structure and morphology (Supporting Information,

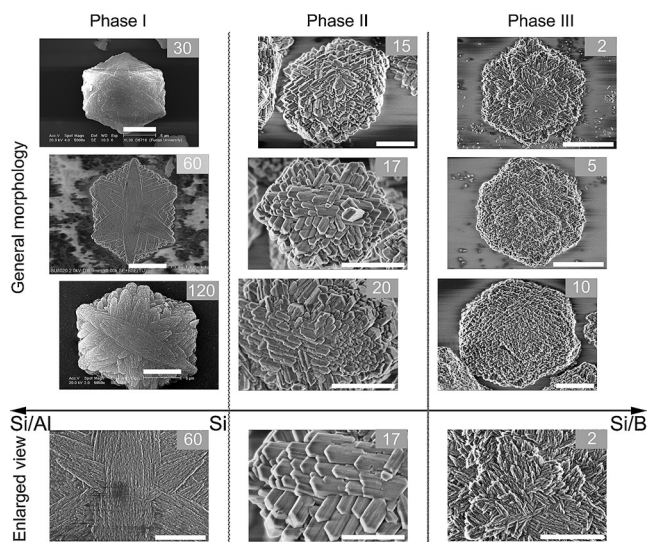


**Figure 1.** Evolution diagram of zeolite MTW under different supersaturations. Top: Phase I: branching growth (Si-Al system, SAR: 30–120, scale bars: 5, 2, and 5  $\mu\text{m}$ ), Phase II: layer-by-layer and branching growth (Si-B system, SBR: 20–15, medium supersaturation, scale bars: all 1  $\mu\text{m}$ ), and Phase III: dendritic growth (Si-B system, SBR: 10–2, high supersaturation, scale bars: 1, 2, and 2  $\mu\text{m}$ ). Bottom: Enlarged view of MTW particles in corresponding phase diagram (scale bars: 2, 0.5, and 1  $\mu\text{m}$ ).

Figures S3–S6 and Table S1): hexagonal shaped plate (Phase I, Si-Al system), numerous nanorods with layer by layer and branching mode (Phase II, Si-B system), and dendritic growth with frequently branching and stacking faults to form a spiral plate (Phase III, Si-B system).

For the zeolites synthesized in the aluminosiliceous system (Phase I; Figure 1), the MTW zeolite is collected when Si/Al ratio in starting gel is higher than 30. The obtained samples mainly present a pseudo hexagonal morphology composed of monoclinic phase of MTW zeolite via Rietveld refinement and related physicochemical analysis (Figure 2a; Supporting Information, Figures S7–S9, Tables S2, S3). From the TEM image (Figure 2b), it can be seen that all particles follow a relative fixed geometry composed of one major and two minor spindle-like prisms with the angular relations of ca.  $65^\circ$  between major and minor branches and ca.  $50^\circ$  for two adjacent minor branches. During the crystallization (Supporting Information, Figures S10, S11), the major prism forms prior to the minor ones, which can be confirmed in a dilute system (Supporting Information, Figure S12). As suggested by electron diffraction (ED) patterns (Supporting Information, Figure S13, Table S4), each prism in the crystal plate extends along its microchannel ([010] direction) and intersects to the adjacent one by sharing ( $hk0$ ) twinning plane. Focused ion beam (FIB) dual beam experiment (Supporting Information, Figures S14, S15) is employed to acquire the interested central thin slice in the hexagonal plate with

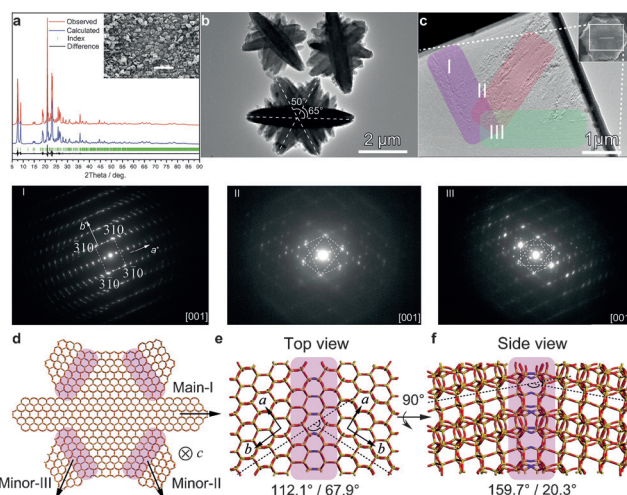


**Figure 2.** Morphology and twinning texture of hexagonal MTW plates. a) Rietveld refinement analysis of MTW twinning structure,  $R_{wp}$  7.54%,  $R_p$  5.44%,  $\chi^2$  1.92, (inset: representative morphology of twinning MTW plate, scale bar: 50  $\mu\text{m}$ ). b) Typical TEM image of hexagonal star composed of three branches with geometry  $4 \times 65^\circ + 2 \times 50^\circ$ . c) Cross-section slice of hexagonal plate; three individual branches are highlighted by different colors (inset: original hexagonal plate). Electron diffraction patterns of twinning boundaries locate at I, II, and III. d) Atomistic projection model of hexagonal star with highlighted twinning boundary (arrows indicate the 1D-12MR channel system, view along  $c$ -axis). e, f) Atomic connectivity profiles of twinning boundary (top and aspect view), respectively.

twinning intersection. The spatial analysis in TEM-EDS experiment on the twinning slice indicates that there is no remarkable elemental difference between the domains and twinning boundaries (Supporting Information, Figure S16, Table S5). In the low-magnification TEM image, the twinning boundary of major and minor branches can be easily discerned by different textures (Figure 2c). The ED patterns of different areas exhibit increasing complexity: from region I (the area of single main trunk) to II (that upon the intersection of the main trunk and a minor intergrown branch) and III (that upon two intersections of the main trunk and two minor intergrown branches). First, in the ED pattern of the main branch locate at region I, only sharp dots from [001] can be obtained (Figure 2c-I). In the ED pattern at region II, apart from the original set of sharp dots of the main trunk, another set of diffraction dots is imposed from the same [001] zone axis but with a rotation angle about  $65^\circ$ , implying that two sets of ED spots overlap along [310], that is, the two adjacent branches intergrow along the specific plane. With respect to the newly formed boundary along the [310], the ED pattern of region II has a  $180^\circ$  rotation around the (310) plane normal (Figure 2c-II). Interestingly, the ED pattern acquired at region III displays the diffraction dots of all of three individual trunk/branches from [001] (Figure 2c-III). Different from the second branch, the third intergrow to the main trunk along  $[3\bar{1}0]$ . Based on anisotropic growth of MTW crystal (Supporting Information, Figure S17), a plausible model can be constructed for pseudo-hexagonal plate with one main trunk and two minor twinning branches sharing a common  $c$ -axis (Figure 2d; Supporting Information, Fig-

ure S18, S19), whose simulated ED patterns (Supporting Information, Figures S18 and S20) are in line with experimental results (Figure 2I, II, III). Its local structure of interface (Figure 2e,f; Supporting Information, Figure S21) shows full atomic connectivity with the  $67.9^\circ$  in (the same as Figure 2b) and  $20.3^\circ$  out of the  $ab$  plane. In the concentrated system, a more complex dendritic morphology with a snowflake-like fractal structure of at least two generations can be clearly identified (Supporting Information, Figure S22), where each branch was interconnected via  $\{310\}$  facets with a common intersection angle of ca.  $65^\circ$ .

By screening the synthesis conditions, MTW fine structure can be deliberately controlled via partial substitution of T atom with boron (Phase II; Figure 1; Supporting Information, Figures S23, S24). It should be noted that the as-synthesized zeolite displays the same hexagonal habitus (Supporting Information, Figure S25). When  $SBR > 10$  in which the system would locate in the medium supersaturation, MTW crystals exhibit the hexagonal plate morphology with layer-by-layer stacking crystalline branches at higher temperature for longer time (Supporting Information, Figure S26). These rod-like branches become thinner and their stacking mode become denser with the increase of boron content (Supporting Information, Figure S27). The phenomena could be anticipated by the Burton–Cabrera–Frank (BCF) theorem,<sup>[10]</sup> in which the crystal growth is governed by mechanisms of dislocation growth, layer-by-layer growth, and fractal growth as increasing supersaturation (Supporting Information, Figure S28).

Furthermore, more detailed structure in each branch could be discerned in the HRTEM image of a microtomed slice cut from hexagonal MTW zeolite plate ( $SBR = 17$ , Figure 3a). The branch has the regular hexagonal shape (Figure 3a, inset), and the stacking faults (SFs) can frequently

appear along the  $c^*$  direction (Supporting Information, Figure S29). The ED pattern (Figure 3b) indicates that the structure is viewed along  $[010]$ . According to the MTW framework, the SFs in the crystals can be attributed to the intergrowth of monoclinic structure with mirror or two-fold operation perpendicular to  $c$ -axis via an intrinsic twinning plane with orthorhombic symmetry and re-aligning to the  $(100)$  plane (Supporting Information, Figure S30, Tables S6, S7). Such structure can be confirmed by consistence of the experimental ED pattern (Figure 3b, taken from the well-ordered microtomed thin slice in Figure 3a) and the reconstructed one (Figure 3c) from the  $[010]$  zone axis of MTW zeolite. The frequent occurrence of SFs along the  $a$ -axis results in the diffuse streaks when  $h \neq 3n$ , while the sharp spots can be observed along the  $[010]_{\text{mono}}$  when  $h = 3n$  ( $n$  is an integer). The phenomena indicate that the intrinsic stacking disorder derives from original monoclinic framework and presents the layer shears of  $\pm 1/3a$ .<sup>[11]</sup> As indicated by structure simulation and electron diffraction, the frequent stacking disorders lead to the appearance of thin layers with orthorhombic symmetry between the monoclinic MTW domains (Supporting Information, Figures S31, S32). For the complex crystallization process of zeolites, the layer by layer stacking structures may derive from multiple pathways of crystal growth involving the oriented aggregation between different crystal domains of MTW.<sup>[12]</sup>

When the crystallization system is turned into a high supersaturation status ( $SBR < 10$ ), different from those in Phase I (Figure 2 and 4a) and II (Figure 3 and 4b) with lower supersaturation, the final plates become a spiral, dendritic structure with main phase of boron-substituted monoclinic MTW (Phase III; Figure 4c; Supporting Information, Figures S33–S39). Combining the SEM and TEM patterns (Supporting Information, Figures S39–S41), the hyper-branching and racemic features can be easily captured. From the further inspection on the HRTEM images along channel direction, the sample exhibits a severely stacking disorder of numerous domains (Supporting Information, Figure S42). Figures 3e and f show the rendered screw dislocation structure of two crystalline layers with different stacking sequences, which derives from the HRTEM results (Supporting Information, Figure S42). Interestingly, it can be seen the layer by layer structures of the zeolite domains along channel direction and their related dim areas (Figure 3d; Supporting Information, Figure S43).

The spiral, hyper-branched structure of Phase III can be recognized as the overlay of above twinning status of MTW zeolite in two different dimensions, that is, 1) the stacking disorder in  $ac$  planes (Figure 3) and 2) the deformation twinning in  $ab$  plane (Figure 2), which construct the screw dislocation core region as the driving force to form this spiral structure in the hexagonal plate (Figure 4). On one hand, as shown in Figure 3e and 4h as an example, the unique stacking disordered structure is bound to break the crystal symmetry in  $ac$  plane (which can also be captured in dense crystal<sup>[1c,d,2]</sup>): 1) first domain (top layer) with even numbered ( $2n$ ;  $n = \text{integer}$ ) SFs (Supporting Information, Figure S44, S45) and 2) the other (bottom layer) without SFs. The top domain with even numbered faults aligns in parallel to the bottom defect-free

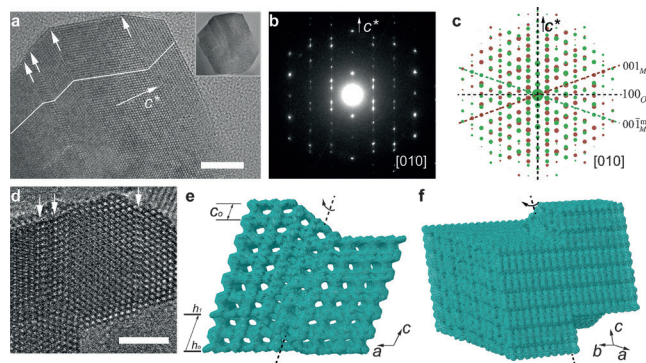


**Figure 3.** Stacking faults in MTW and related screw dislocation core structure. a) HRTEM image of the thin slice, arrows indicate the SFs position and the trace line presents the crystal growth direction (scale bar: 20 nm, inset: the intact cutting slice, thickness ca. 40 nm). b) Rotated ED pattern of intact thin slice in inset of (a). c) Reconstructed ED pattern: the dash lines mark the principal direction for monoclinic phase along the  $[010]$  zone axis. d) HRTEM image of screw dislocation structures, arrows marks the fuzzy area resulted from superimposition of bilayer with different SFs; scale bar: 10 nm. e, f) Rendered 3D atomistic model of screw dislocation core ( $C_0$ : unit parameters along  $c$ -axis,  $h$ : spiral pitch, detailed atomistic framework is shown in the Supporting Information, Figure S42).

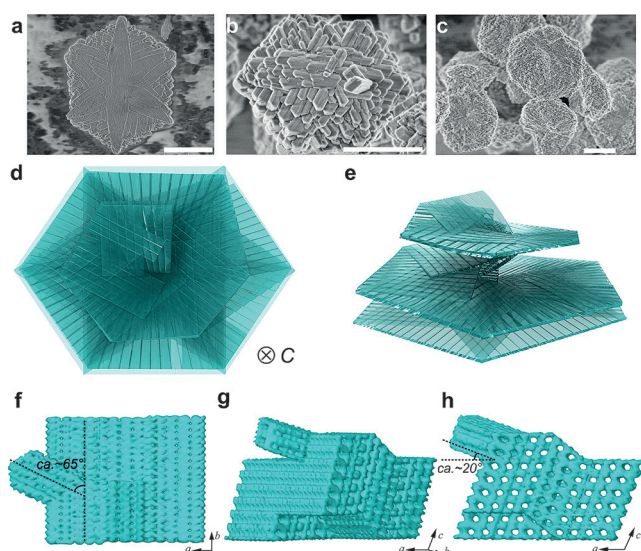


**Figure 4.** Collaborative growth behaviors along two different directions in MTW zeolite. a)–c) Representative structure in MTW under increasing supersaturation (a: SAR = 60, b: SBR = 17, c: SBR = 2), scale bar: 5, 1, and 2  $\mu\text{m}$ . d), e) General structure of the fractal spiral structure of MTW. f), g) Rendered atomic model of the two independent growing dimensions in MTW structure observed from different directions (Detailed atomistic framework is deposited in the Supporting Information, Figure S48).

domain in starting and ending parts owing to the same stacking vector (Supporting Information, Figures S46, S47). An intact Burgers circuit is thus formed<sup>[13]</sup> for exertion of the screw dislocation structure (Figure 3 e,f) with a regular spiral pitch  $h = nC_0$  ( $n$ , integer number;  $C_0$ ,  $1/2$  unit parameters along  $c$ -axis). On the other hand, the deformation twinning at (310) plane leads the generation of the branches with screw angle ( $\theta$ ) of  $67.9^\circ$  in  $ab$  plane and spatial angle ( $\psi$ ) of  $20.3^\circ$  out of the  $ab$  plane (Figure 4 f–h) referred to in Figure 2. These two factors are the structural foundation of the spiral, hyper-branched structure of Phase III, and the collaborative growth behavior in two dimensions generates fractal spiral structure. With increase of boron content, the prisms in the hexagonal plate particles appear more frequently with smaller size to form a dendritic pine-tree-like branches in  $ab$  plane. Furthermore, the frequent 2D nucleation events on the plates bring about the frequent appearance of SFs along  $a$ -axis (looking down  $ac$  plane) to form the screw dislocation core region with numerous fragments (Supporting Information, Figure S48), which further promotes fractal growth in the  $ab$  plane by fast extension along the channel direction and facilitates the continuous self-iteration process.

Such screw dislocation structure creates inner strain ( $E_{\text{strain}}$ ) in the periodic crystalline lattice. According to the elastic theory, the stress field exerts a torque throughout the whole plate at the central area, and the strain energy depends on the magnitude  $E_{\text{strain}} \propto \mathbf{b}^2$  (where  $\mathbf{b}$  is the Burgers vector). The phenomena were often observed in dislocation-driven dense phase materials, such as ZnO nanotubes or  $\text{Bi}_2\text{Se}_3$  plates.<sup>[1c,d]</sup> An energy balance between surface energy  $2\pi r\gamma$  ( $\gamma$ , surface energy) and inner strain  $E_{\text{strain}}$  can be disturbed,

and the solid plate becomes hollow, as is confirmed here (Supporting Information, Figures S49–S51).

The above conceptual evolution model of spiral structure of MTW also can be adopt to interpret those in the nanoporous materials with different topology. For a known screw dislocation, there must be a nucleation in the plane and a spread along the vertical direction in the crystal, which involves the two collaborative growth behaviors along the two different dimensions. As previously reported spirals in nanoporous systems, such as LTA<sup>[7,14]</sup> (Supporting Information, Figure S52, Table S8), CHA/AEI,<sup>[15]</sup> STA-7 (SAV),<sup>[16]</sup>  $\text{ZnPO}_4$ -Sodalite, and  $\text{ZnPO}_4$ -Faujasite,<sup>[17]</sup> 3D spiral terraces are considered here to be defined by three crucial parameters: spiral pitch  $h$ , screw angle  $\theta$ , and spatial angle  $\psi$ . For LTA zeolite, the above two angles are  $90^\circ$  and  $0^\circ$ , respectively. In the each corner of the LTA square spiral terrace, the adjacent segments rotate about  $90^\circ$  and fuse into the bulky crystal owing to the identical atomic arrangement in the (010) and (001) planes. It worth noting that other nanoporous materials with a high level of symmetry always fuse into their bulky crystal and leave a spiral terrace on the surface owing to the overlap of two dimensions, which may explain that why we seldom capture the screw dislocation structure in the nanoporous system.<sup>[7,18]</sup> In MTW zeolite with lower symmetry ( $C2/c$ ), the three parameters are determined as spiral pitch: 1.2 nm, screw angle:  $67.9^\circ$  with spatial angle:  $20.3^\circ$ , and the layer by layer stacked branches aggregate into a pine-tree-like, spiral contour on the original hexagonal plane. In contrast to the regular spiral terrace on the flat zeolite surface,<sup>[13–16]</sup> it is hard to obtain the regular spiral step height on the highly dendritic surface structure of MTW (equal to the Burgers vector along the vertical direction) by atomic force microscopy, but the spiral patterns and hillocks can still be clearly recognized.

In summary, we proposed the conceptual structural model of MTW zeolite spiral plates driven by the screw dislocation region, which is confirmed by the features of surface spiral contours, screw dislocation core, and hollow core structure. Different from nanoporous materials with high symmetry (for example, CHA/AEI,<sup>[15]</sup> SiC ceramic<sup>[2,19]</sup>), the special growth mode in this MTW zeolite plate involves the collaborative manner of frequent intergrowth along (310) plane and propagation of SFs along the vertical dimension. The dimensional change of nanosized zeolite rods via iterative deformation twinning and intrinsic intergrowth procedure is a novel strategy toward hierarchical materials with interconnected abundant pore structures (Supporting Information, Figures S53–S55). This strategy might be applied to other zeolite structures that can 1) derive a novel zeolite phase by regular extension of deformation twinning boundary (Supporting Information, Figure S56) and 2) offer a potential opportunity to distinguish the end-polymorph from hybrid phases (Supporting Information, Tables S6, S7). Furthermore, such a zeolite with confirmed complex twinning and stacking faults were confirmed with an enhanced catalytic performance owing to its textural and framework properties (Supporting Information, Figures S57, S58).

Additionally, the model for polymorph intergrowth in this work is totally different from the known models that

developed for MFI/MEL and FAU/EMT systems. For MFI/MEL, the central MEL node with higher symmetry plays as direct connector with lower symmetrical MFI nanosheets to form self-pillared pentasil.<sup>[5]</sup> For FAU/EMT, the random EMT nuclei intergrow with FAU nanosheets to break the cubic symmetry and form a hierarchical structure.<sup>[6]</sup> The orthorhombic polymorph in the screw dislocation of MTW zeolite only acts as a bridge to change the relative position along the screw dislocation circuit, and can be manipulated by supersaturation. The unique phenomena also provide a novel vision to understand the polymorph intergrowth and its role in the architectural evolution of zeolite. Varying from the exact fractal patterns by mathematical expressions, the fractal pattern in practice is statistically self-similar and evolves under certain circumstance with time. Essentially, the fractal system depends on the two crucial factors: units with self-similarity and a dynamic iteration procedure. The present fractal pattern is self-organized by branching and intrinsic twinning to construct a hierarchal dissipative structure under the domination of energy.

### Acknowledgements

This work was supported by National Key Basic Research Program of China (2013CB934101) and NSFC (21433002, 21573046, 21473037, and U1463206). We thank Dr. J. L. Sun (Peking University) for helpful suggestions on disordered structures and Dr. P. Guo (DICP) for thoughtful discussions. We thank G. R. Zhou for cutting thin slices of the samples for HRTEM observation. Special thanks are due to reviewers for many helpful comments.

### Conflict of interest

The authors declare no conflict of interest.

**Keywords:** coincidence boundaries · fractal patterns · crystal intergrowth · structure evolution · zeolites

**How to cite:** *Angew. Chem. Int. Ed.* **2017**, *56*, 11764–11768  
*Angew. Chem.* **2017**, *129*, 11926–11930

- [1] a) M. J. Bierman, Y. K. A. Lau, A. V. Kvit, A. L. Schmitt, S. Jin, *Science* **2008**, *320*, 1060–1063; b) J. Zhu, H. Peng, A. F. Marshall, D. M. Barnett, W. D. Nix, Y. Cui, *Nat. Nanotechnol.* **2008**, *3*, 477–481; c) S. A. Morin, M. J. Bierman, J. Tong, S. Jin, *Science* **2010**, *328*, 476–480; d) A. Zhuang, J.-J. Li, Y.-C. Wang, X. Wen, Y. Lin, B. Xiang, X. Wang, J. Zeng, *Angew. Chem. Int. Ed.* **2014**, *53*, 6425–6429; *Angew. Chem.* **2014**, *126*, 6543–6547.

- [2] S. Harada, K. Seki, Y. Yamamoto, C. Zhu, Y. Yamamoto, S. Arai, J. Yamasaki, N. Tanaka, T. Ujihara, *Cryst. Growth Des.* **2012**, *12*, 3209–3214.
- [3] F. Ding, A. R. Harutyunyan, B. I. Yakobson, *Proc. Natl. Acad. Sci. USA* **2009**, *106*, 2506–2509.
- [4] K. Thuermer, S. Nie, *Proc. Natl. Acad. Sci. USA* **2013**, *110*, 11757–11762.
- [5] a) X. Zhang, D. Liu, D. Xu, S. Asahina, K. A. Cychosz, K. V. Agrawal, Y. Al Wahedi, A. Bhan, S. Al Hashimi, O. Terasaki, M. Thommes, M. Tsapatsis, *Science* **2012**, *336*, 1684–1687; b) D. Xu, G. R. Swindlehurst, H. Wu, D. H. Olson, X. Zhang, M. Tsapatsis, *Adv. Funct. Mater.* **2014**, *24*, 201–208.
- [6] M. Khaleel, A. J. Wagner, K. A. Mkhoyan, M. Tsapatsis, *Angew. Chem. Int. Ed.* **2014**, *53*, 9456–9461; *Angew. Chem.* **2014**, *126*, 9610–9615.
- [7] A. M. Walker, B. Slater, J. D. Gale, K. Wright, *Nat. Mater.* **2004**, *3*, 715–720.
- [8] W. Vermeiren, J.-P. Gilson, *Top. Catal.* **2009**, *52*, 1131–1161.
- [9] a) S. Ritsch, N. Ohnishi, T. Ohsuna, K. Hiraga, O. Terasaki, Y. Kubota, Y. Sugi, *Chem. Mater.* **1998**, *10*, 3958–3965; b) I. Kinski, P. Daniels, C. Deroche, B. Marler, H. Gies, *Microporous Mesoporous Mater.* **2002**, *56*, 11–25.
- [10] a) W. K. Burton, N. Cabrera, F. C. Frank, *Philos. Trans. R. Soc. London Ser. A* **1951**, *243*, 299–358; b) *Crystal Growth for Beginners*, 2nd ed., World Scientific, Singapore, **2011**, pp. 1–75.
- [11] a) M. Moliner, J. González, M. T. Portilla, T. Willhammar, F. Rey, F. J. Llopis, X. Zou, A. Corma, *J. Am. Chem. Soc.* **2011**, *133*, 9497–9505; b) T. Willhammar, J. Sun, W. Wan, P. Oleynikov, D. Zhang, X. Zou, M. Moliner, J. Gonzalez, C. Martínez, F. Rey, A. Corma, *Nat. Chem.* **2012**, *4*, 188–194.
- [12] J. J. De Yoreo, P. U. P. A. Gilbert, N. A. J. M. Sommerdijk, R. L. Penn, S. Whitlam, D. Joester, H. Zhang, J. D. Rimer, A. Navrotsky, J. F. Banfield, A. F. Wallace, F. M. Michel, F. C. Meldrum, H. Cölfen, P. M. Dove, *Science* **2015**, *349*, aaa6760.
- [13] R. L. Penn, J. F. Banfield, *Science* **1998**, *281*, 969–971.
- [14] S. Dumrul, S. Bazzana, J. Warzywoda, R. R. Biederman, A. Sacco, Jr., *Microporous Mesoporous Mater.* **2002**, *54*, 79–88.
- [15] R. L. Smith, W. A. Slawinski, A. Lind, D. S. Wragg, J. H. Cavka, B. Arstad, H. Fjellvag, M. P. Atfield, D. Akporiaye, M. W. Anderson, *Chem. Mater.* **2015**, *27*, 4205–4215.
- [16] P. Cubillas, M. Castro, K. E. Jelfs, A. J. W. Lobo, B. Slater, D. W. Lewis, P. A. Wright, S. M. Stevens, M. W. Anderson, *Cryst. Growth Des.* **2009**, *9*, 4041–4050.
- [17] P. Cubillas, M. W. Anderson, *Zeolites and Catalysis*, Wiley-VCH, Weinheim, **2010**, pp. 1–55.
- [18] R. L. Smith, A. Lind, D. Akporiaye, M. P. Atfield, M. W. Anderson, *Chem. Commun.* **2015**, *51*, 6218–6221.
- [19] J. Hassan, J. P. Bergman, A. Henry, E. Jánzén, *J. Cryst. Growth* **2008**, *310*, 4424–4429.

Manuscript received: May 2, 2017

Revised manuscript received: June 29, 2017

Accepted manuscript online: July 20, 2017

Version of record online: August 21, 2017